Synthesis and Structural Evolution of Dual-Boron-Source-Modified Polysilazanes Derived SiBCN Ceramics

Journal:	*New Journal of Chemistry*
Manuscript ID	NJ-ART-12-2015-003723.R2
Article Type:	Paper
Date Submitted by the Author:	02-Jun-2016

Complete List of Authors:	Zhang, Qian; Institute for Advanced Ceramics, material science and engneering Yang, Zhihua; Harbin Institute of Technology, Jia, Dechang; Institute for Advanced Ceramics, Chen, Qingqing; Harbin Institute of Technology Zhou, Yu; Harbin Institute of Technology,

New Journal of Chemistry

ARTICLE

Synthesis and Structural Evolution of Dual-Boron-Source-Modified Polysilazanes Derived SiBCN Ceramics

Received 00th January 20xx,
Accepted 00th January 20xx

DOI: 10.1039/x0xx00000x

www.rsc.org/

Qian Zhang, Zhihua Yang,* Dechang Jia,* Qingqing Chen and Yu Zhou

We demonstrated here a novel synthesis of polyborosilazane (PBSN) precursor using hydroboration and aminolysis reaction synergies to modify a polysilazane (PSN). Specifically, borane·tetrahydrofuran and boron trichloride·hexane were used as dual boron sources, which not only reacted with Si–Vi and Si–N–H functionality respectively to modify multiple active sites of PSN resulting in boron-rich silicon-boron-carbide-nitride (SiBCN) ceramics, but also improved controllability on composition, molecular structure, as well as final features. The resulting structures were characterized by FTIR, solid-state ^{11}B and ^{29}Si magic-angle-spinning NMR and inductively coupled plasma emission spectral (ICP) analysis. These polymers were found to be structurally complex networks composed of tri-coordinate BC_xN_{3-x} and tetra-coordinate BC_xN_{4-x} bridges. The resulting polyborosilazanes contained ~11 wt% higher boron contents than that in the starting polymer. The structural evolution of the resulting polymers was evaluated by means of XPS, FTIR and XRD, and TGA-DSC-QMS was utilized to detail the precursor-to-ceramic.

Introduction

Polymer-derived ceramics (PDCs), especially the introduction of silicon nitride/silicon carbide (Si_3N_4/SiC) and silicon boron carbide nitride (SiBCN), have been widely studied over the past 50 years. Part of the motivation was the utility of being able to preform shapes using polymer processing techniques and another one was due to the good-to-excellent thermal, mechanical and chemical stability at high-temperatures of the resulting ceramics.[1] Multiple applications have been developed in various fields including high-temperature-resistant materials and functional materials in electrical engineering as well as in nanoelectronics.[2] Researchers have found that PDCs can be functionalized through the incorporation of boron into the system in pursuit of materials with excellent high temperature performance. Since boron inhibits the SiC crystallization and suppresses the decomposition of Si_3N_4 to improve the thermal stability of SiBCN ceramics,[3] the tunable boron content is significant for SiBCN ceramics by limiting crystallization and reducing sensitivity to oxidative degradation.

Because of the 3D structure inherent in quaternary SiBCN ceramics, the carbon is much less susceptible to oxidation and such networks also retard the diffusion that would lead to crystallization.[4] These distinct advantages of SiBCN ceramics over traditional PDCs inspired improving them resulting in much improved strengths and thermal stability with respect to oxidation and crystallization. Therefore, most work has targeted such materials for their applications in extreme environments including fibers used in composite,[5] membranes and related ultrahigh temperature materials.[2e,6] These properties arise primarily because of the unique amorphous structures provided by SiBCN ceramics that depend on the chemical structure of the polymer precursors along with methods of processing.[7]

Although various existing methods to obtain boron-containing polymer presursors, the mechanism is mainly divided into the following classes. Firstly, the boron is introduced poly or oligo-silazanes typically by aminolysis polymerization of boron-containing monomers possessing Si–Cl or B–X (X=Cl and Br) in the presence of NH_3 or polysilazane monomers.[8] Secondly, the hydroboration of unsaturated groups (e.g. vinyl groups and hydrogen) in Si-based polymers with monofunctional or multifunctional boranes is also developed to synthesize boron-containing polymers, since the pioneering work of Riedel *et al*. are published.[9] Alternatively, Si-based precursor polymers could react with borane derevatives *via* dehydrogenative coupling reactions.[10] As a further simplification, hydroboration of polysilazanes with vinyl-terminated is utilized after ammonolysis of chlorosilanes to eliminate the by-product. In almost all methods developed

Institute for Advanced Ceramics, School of Materials Science and Engineering, Harbin Institute of Technology C3#- Room 516, No. 2, Yikuang Street, Nangang District, Harbin 150001, PR China.E-mail: dcjia@hit.edu.cn (Jia D.C.); *zhyang@hit.edu.cn (Yang* Z.H.)

† Electronic Supplementary Information (ESI) available: Fig. S1 X-ray diffraction (XRD) of the by-product of PBSN2, Fig. S2 Thermogravimetric analysis of precursor polymers PSN, PBSN1 and PBSN2, Fig. S3 TGA-QMS spectra of PSN, Fig. S4 TGA-QMS spectra of PBSN1, Fig. S5 TGA-DTG curves of liquid PBSN2 before thermal curing. Fig. S6 Elemental XPS spectra of PBSN1 pyrolyzed at varied temperatures.

for synthesis of SiBCN precursor polymers, it is unavoidable to involve special handling of hazardous chemicals (ammonia, chlorosilazanes and pinacolborane) and their by-products.[11]

On the other hand, SiBCN precursor polymers involve the aminolysis polymerization of boron-containing monomers and aminolysis of chlorosilazanes with boranes such as the borane dimethyl sulphide complex ($BH_3{\cdot}SMe_2$) resulting in a low boron retention in the final ceramics.[12] Recently, Sarkar *et al*. explored the hydroboration modification of polyborosilazane with borane which give rise to precursors with high ceramic yields of 85 wt%.[9c] Thus, polymer routes to organosilazane polymer or oligomers with large boron contents are simply and effectively available, highlighting its potential for the research in this field.[13] However, controllability on composition, conversion and yield of precursor polymers, availability and environmental protection are considerable in this case, due to the necessity of active ammonia (such as NH_3 or methylamine) in the process of preparing such SiBCN ceramics.

In the routine preparation of molecular sieves, structure directing agents (SDA) are crucial for the synthesis of compounds with specific structures. The use of two types of SDAs can also be of considerable advantage for some zeolitic structures, which is known as dual-template approach.[14] Inspired by the fact that the properties can be adjusted using different ligands, we report here efforts to explore the use of two different boron sources to regulate connectivity in SiBCN ceramics precursors with the major objectives of controlling boron contents, precursors and ceramic product properties.

In this contribution, tunable boron contents quaternary SiBCN ceramics with uniform boron dispersion are prepared by pyrolysis of controllability polyborosilazane precursors. A novel dual-boron source approach is utilized to tune the boron contents of polyborosilazanes precursors based on a combination of the aminolysis reaction of BCl_3·hexane with the Si–NH groups and the hydroboration modification of Si–C=C functional groups in polysilazane with BH_3·THF, to form Si–N–B chains with Si–C–B cross-links. Actually, the BNC2 structure is stable in comparison to BC3 structure. This specific dual-boron-source method promises the potential to tailor the nitrogen with boron and significantly influenced the molecular structure of the final ceramics, which represents a convenient approach to SiBCN ceramic materials with high boron content and thermostability. As we will show below, the boron concentrations are effectively increased to resist the crystallization in the resultant SiBCN ceramics additive-free ammonia as the nitride source, as well as any catalyst.

Experimental Section

Materials

Borane tetrahydrofuran complex and triethylamine (TEA) were purchased from Sigma-Aladdin reagent (Shanghai, China), boron trichloride (BTC) was purchased from Rui He Chemical Sci. and Tech., Guangzhou, china). All reagents have been dewatered to anhydrous reagents. Polysilazane was prepared according to the reported method.[15]

Characterization

Fourier transform infrared Spectroscopy (FTIR) data were recorded on a Perkin-Elmer Spectrum One spectrophotometer with sample as KBr disks in the range of 4000–450 cm^{-1}. Further, thermal analysis was carried out by TGA-DSC-MS (and TGA-DTG) (Q100/ STA449C, Germany, NETZSCH) at a temperature range from 30° to 1550 °C in argon atmosphere. Powder X-ray diffraction (XRD) data were recorded on a Rigaku D/Max-3B X-ray diffractometer with Cu$K\alpha$ as the radiation source (λ = 0.145 nm) in the angular range 2ϑ = 10°–90° at room temperature. The connecting way of chemical bonds and element content of PSN, PBSN1 and PBSN2 was characterized by X-ray photoelectron spectroscopy (XPS, Kratos, ULTRA AXIS DLD) with Al (monochrome) Kα radiation at the pass energy of 1486.6 eV. All binding energies were calibrated by referencing to C 1s (284.6 eV). ICP was carried out by ICP-ASE (Agilent ICP-OED720, Australia) to analyse boron and silicon content after digestion of the samples in a mixture of HF-HCl-HNO_3, and Elemental analysis was carried out by Vatio Mactro cube (Elementar, Germany) for nitrogen element. All ^{29}Si, and ^{11}B MAS NMR spectra were collected using a Bruker AVANCE III 400 WB solid-state spectrometer (Bruker Biospin, Billerica, MA) operating at the Larmor frequencies of 79.5 and 128.4 MHz, respectively, for these nuclide. Crushed samples were loaded in ZrO_2 rotors under argon and spun at a rate of 5 kHz using a 4-mm double resonance MAS probe, respectively. NMR chemical shifts were externally referenced to tetramethylsilane for ^{29}Si, trimethyl borate for ^{11}B.

Results and Discussion

A novel boron-modified polysilazane precursor for the SiCBN ceramics fabrication was synthesized upon the PSN-based polymer containing Si–Vi (–CH=CH_2) and Si–H groups (PSN = polysilazane). PSN was chemically modified by BH_3·THF reacted with Si–Vi within PSN at the first step. A small amount of Si–N groups may react with BH_3 at the same. Secondly, the BCl_3·hexane could further react with the N–H within PSN. PSN as Lewis base attacked to as BTC Lewis acid, that meant –Si–NH–SiNH of PSN reacted with B–Cl of BTC, and then carried on with increasing chains through condensation. Finally, the two novel SiBCN ceramic precursors were successfully prepared, the routine preparation of boron-modified polysilazanes precursors were shown in Scheme 1.

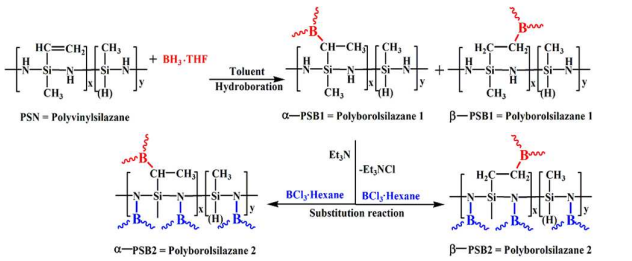

Scheme 1 Synthesis pathway of PSN modified with BH_3·THF and BCl_3·hexane.

Synthesis of PSN, PBSN1 and PBSN2

All reactions were conducted under the high purity and dry argon using standard Schlenk techniques. A toluene solution (40 mL) of 12.0 g (15 mmol) poly(vinylmethyl)-co-poly(hydro)silazane (PSN) and 15 mL (15 mmol) borane tetrahydrofuran complex was added into a 300 mL two-necked Schlenk flask equipped with Ar inlet and magnetic stirrer. The mixture was stirred for 4 h at 0 °C using ice-salt baths. Then, 15 mL (15 mmol) boron trichloride was slowly added dropwise and the clear solution was further stirred for 6 h. A white precipitate was generated and the viscosity of polymer solution was increased, when we droped the BCl_3 into the PBSN1 solution. In this process, the ratio of reactants (BCl_3:Et_3N) was 1:3(mole) and the Et_3N worked as acid binding agents. Insoluble trimethylamine hydrochloride as the by-product was removed by filtration, and the solvent distilled off under vacuum (Fig. S1). The quality of the by-product was almost consistent with the design stoichiometric ratio. Mass fraction: PSN: Si, 41.8 wt%. PBSN1: Si, 37.7; B, 4.2 wt%. PBSN2: Si, 34.9 wt%; B, 11.1 wt%.

The final viscous liquid was immediately cured at low temperature owing to its temperature-sensitivity by heating to 120 ° – 190 °C (PSN: 130 °; PBSN1: 160 °; PBSN2: 190 °C) with a dwell time of 3 h under Ar. The heating temperatures were chosen due to the curing temperatures of PSN, PBSN1 and PBSN2 (120 °, 150 ° and 180 °C), respectively as can be seen from the DTG curves in Fig. S5. Heating promotes polycondensation as evidenced by gradual increases in viscosity. On curing to a solid, a chemically stable product was obtained.

Preparation of SiBCN Ceramics

To investigate SiBCN crystallization, a series of precursors with different boron contents were pyrolyzed under Ar in a corundum tube furnace (RHTH 120-600/18, Nabertherm Corporation, Germany) at 800 °, 1100 °, 1400 ° and 1600 °C, respectively. Pyrolysis were run at a heating rate of 5 °C·min^{-1} with a 2 h dwell time.

Synthesis of Polyborosilazanes by Dual-Boron-Source Method

The PBSN1 and PBSN2 were synthesized via a dual-boron-source approach to tune the boron contents of polyborosilazanes. The ^{29}Si and ^{11}B MAS NMR spectra of a series of resulting polyborosilazanes were presented in Fig. 1 and Fig. 2, respectively. ^{29}Si CPMAS spectra were collected using p/3 (2.6 μs) rf pulses and 60 s recycle delay. Each ^{29}Si spectrum was obtained through Fourier transformation and approximately 2000 free inductions decays (FIDs) were averaged. ^{11}B MAS NMR spectra was collected with a p/12 pulse length of 0.2 μs and a recycle delay of 0.2 s. Approximately 160 FIDs were collected and averaged to obtain each ^{11}B MAS NMR spectrum.

The ^{11}B and ^{29}Si NMR spectra confirmed the silicon hydrogen bonds with a proton resonance at 4.42 ppm and branched structures. The schematic route followed for this study is illustrated in Fig. 1 and Fig. 2. The PSN can be obtained cross-linked networks structure from condensation polymerization and hydrosilylation below 200 °C that have been studied previously.

The ^{29}Si CPMAS NMR spectra of the PSN, PBSN1 and PBSN2 are shown in Fig. 1. The ^{29}Si spectra of the PSN contains mainly one heterogeneously widely Gaussian peak with a ^{29}Si isotropic chemical shift (δ_{iso}) of ~ -23.4 ppm, typical values for tetrahedral Si in $SiHCN_2$ tetrahedra, as seen in similar polymers.[16] The broad primary peak is indicative of Si atoms in amorphous structures. In addition, a minor peak at -18 ppm can be attributed to $SiHC_2N$ units.[17] Although the resonances are dominated by broad peaks around -23.4ppm, the signal is asymmetric with two shoulders near -5.7 and -36 ppm characteristic of small amounts of SiN_2C_2 and $SiCN_3$, respectively.

Likewise, the ^{29}Si CPMAS NMR spectra of polymers PBSN1 and PBSN2 also reveal similar broad peaks with resonances from -5 to -40 ppm centred near -15 and -30 ppm, respectively, which correspond to the presence of mixtures of SiC_xN_{4-x} tetrahedra. However, the PBSN2 and PBSN1 ^{29}Si NMR signals have slight shifts to the high-field compared with PSN that suggest $SiH_zC_xN_y$ (x+y+z=4) species, likely indicative of boron bonded with $SiH_zC_xN_y$ (x+y+z=4) tetrahadra decreasing electron density at Si. Peaks around -5.5, -21.7, -26.4 and -35 ppm can be assigned to SiN_2C_2, $SiHC_2N$, $SiHCN_2$ and $SiCN_3$, respectively, also appear to be presented in PBSN1. Their positions coincide with the reference SiN_2C_2 and $SiHCN_2$ indicating similar SiN_2C_2 and $SiCN_3$ structural units in both networks. Furthermore, the shoulders on the SiC_2N_2 peak suggest the presence of small concentrations of SiN_2C_2 tetrahedra in the samples. This indicates the formation of an amorphous SiCN ceramic phase

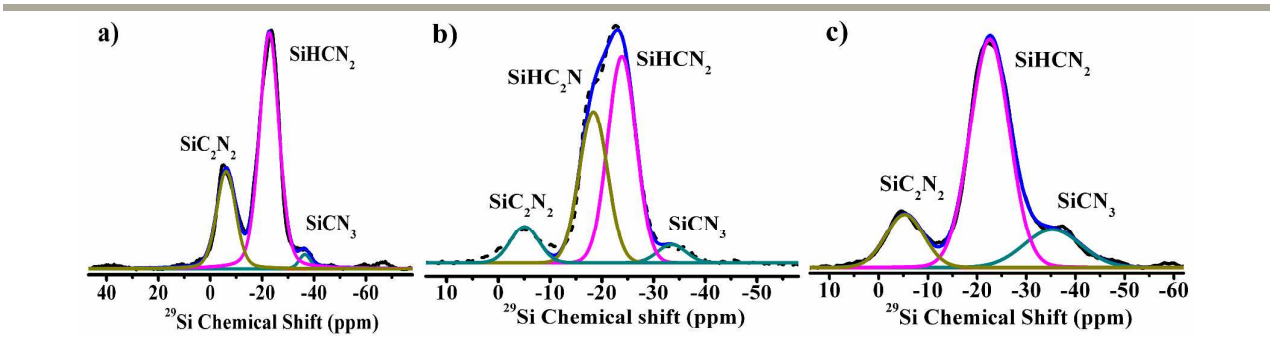

Fig. 1 Solid state ^{29}Si CPMAS NMR spectrum recorded for PSN (a), PBSN1 (b) and PBSN2 (c) curing at 190 °C.

with heterogeneity in the local environment around the Si atoms, which is identical to the initial polymer-derived ceramic product.[18]

Compared with PBSN2, ^{29}Si NMR spectra of PBSN1 depicts that the amount of SiN_3C decreases because of the aminolysis reactions and methane release, which has been reported.[19] The slightly differences in chemical shift point were due to the rearrangements of polymer backbone occurred and $SiHC_2N$ units disappeared. Peaks of SiN_3C decrease obviously with the reaction between boron and N–H to break Si–NH bonds as a consequence of the curing process.

The ^{11}B MAS NMR spectra of PBSN1 and PBSN2 are similar (no resonance signal observed in PSN) as seen in Fig. 2. Experimental ^{11}B MAS spectrums are dominated by the excitation of the central m_I = -1/2 ~ +1/2 transition. Due to the large heterogeneity in the local chemical environment of the boron nucleus, ^{11}B NMR spectra usually exhibit distinct second order broad and featureless peaks, even with MAS spinning. That means the boron nuclei are found in both tetrahedral and trigonal coordination. We make a general assumption that the B atoms are presented in variable amounts of B–N, B–C and B–H bonds, giving rise to a large distribution of quadrupolar coupling constants, as reflected by the ^{11}B NMR spectra.

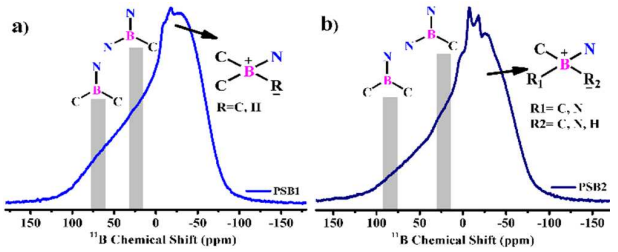

Fig. 2 Solid state ^{11}B MAS NMR spectra of PBSN1 (a) and PBSN2 (b) curing at 190 °C, that the chemical shift ranges expected for BC_xN_y (x+y ≤ 4). Sample rotation frequency: 5 kHz.

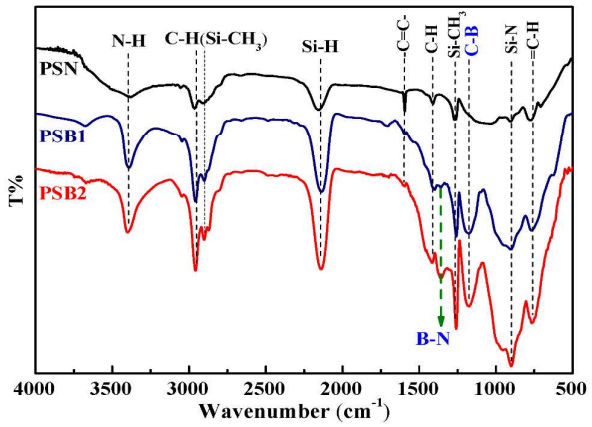

Fig. 3 FTIR spectra of PSN and boron-modification of polysilazane cross-linked at 200 °C for 3 h.

According to the proposed structures for each system, BCH_2–, BCN_2–, and BN_3– coordination environments, tri-coordinated boron is presented, and the solid NMR ^{11}B data suggest that the replacement of a B–N by a B–C bond should give rise to a downfield shift in the ^{11}B resonance.

The ^{11}B isotropic chemical shifts can be fit with six Gauss peaks 77, 40, 29.7, 1, -30 and -40 ppm, respectively. These resonances with δ_{iso} near 80, 44 and 29.7 ppm agree well with the formation of BC_3 units as $B(CH)_3$, BCN_2 in $(C_2H_4)_2B$–$[(NH)SiCH_3]$ and BN_3.[20] Moreover, the three peaks at -1, -13 and -48 ppm correspond to the formation of C_3BN species formed through lone-pair electron N coordinated with electron-deficient B.[8] The amine-borane bond in trialkylboron can be formed in the presence of amine at temperature of 110 ° – 180 °C without catalysts.[6b]

The formation of $BNC_{2(sp3)}$ can be attributed to C–B–C and H–N are broken and H atoms attach to –Vi groups with minimum steric hindrance to form the amine-borane bond. Meanwhile, the SiC_2N_2 units can be traced to the strong affinity of the boron to bind nitrogen reaction scheme in Eq (1) and Eq (2). $–BH_2$ of the $(CH)BH_2^+$, $(CH_2)BH_2^+$ and BC_xN_{3-x} chains, respectively, are seen and appeared similar to that reported previously in ammonia borane.[21]

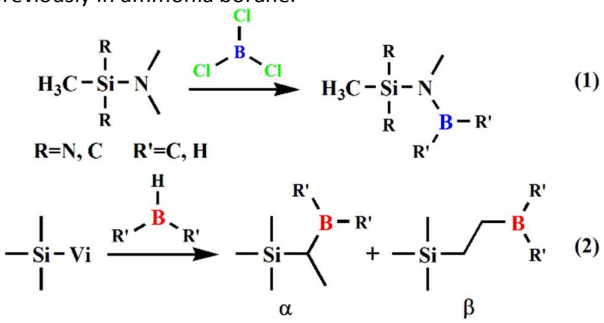

The solid-state ^{11}B NMR indicated that boron environment in both resulting polymers was more complicated than expected as illustrated in Fig. 2. Obviously, PBSN2 forms with H_2 release as evidenced by $–BH_2$ and –BH species. The other tetra-coordination boron such as BCN_3 was formed by the reaction mechanism of the borane electrophile substitution that contributes to $–BC_xN_{4-x}$ units. This was a common structural feature in this type of polymer.

The aforementioned high-field signal at -1, -30 and -48 ppm are attributed to $BC_{4-x}N_x$ where boron is not protonated, and are found in boron-modified polysilazanes obtained by aminolysis.[17] It is worth noting that we can determine the exact nature of tetra-coordinated boron precisely, in terms of synthesis and previous NMR observations. This result clearly emphasizes that the chemical composition and architecture of precursor polymers have a crucial effect on the phase composition of the resulting ceramic.[14a] Conversely, the

structure of polyborosilazanes is characterized by significant mixed bonding in form of the appearance of BN_xC_y ($x+y \leq 4$) triangle and tetrahedra, owing to the distinct boron-sources coordinated with the silicon-nitride backbone. Further, residual −H was observed after cross-linking. We can also observe a slight different structure between PBSN1 and PBSN2, even more evidence should be provided. FTIR spectra of these precursor polymers (Fig. 3) support this finding. The absorption assigned to C–B–C and B–N, respectively, at the same time.[17]

Table 1 The theoretical calculating (tt.) and actual weight (ac.) value of chemical compositions (by wt.%) of PBSN1 and PBSN2 cross-linked at 200 °C.

Sample	Si[a]		B[a]		N[b]	
	tt.	ac.	tt.	ac.	tt.	ac.
PSN	34.44	34.6	0	0	24.10	25.2
PBSN1	30.33	30.4	6.84	5.9	22.69	23.2
PBSN2	24.57	25.0	18.29	17.8	18.38	18.6

[a]: Measured by ICP-AES.
[b]: Measured by elemental analyzer Vario Macro cube.

In more detail, the part of chemical compositions of PBSN1 and PBSN2 cross-linked at 200 °C were measured by atomic spectroscopy method. The results of ICP-AES are shown in Table 1.

Structural Evolution of the Precursors

FTIR is used to investigate structural evolution of the precursor, comparing PSN with PBSN1 and PBSN2. In cross-linked PSN, typical absorption bands relates to *v*SiC–H (2957, 2905 cm^{-1}), *v*SiN–HSi (3395 cm^{-1}), *v*Si–H (2137 cm^{-1}) and δSi–N (1021–945 cm^{-1}) groups are observed as shown in Fig. 3. The observations of weaker bands at 1592 cm^{-1} and 3053 cm^{-1} for the vinyl units in PBSN1 reveal the hydroboration of C=C bonds followed the Markov's rules. Meanwhile, it further confirms the above results through the emergence of the stretching vibrations for B–C at 1176 cm^{-1} and B–N bond at 1403 cm^{-1}.

After heat-treatment at 140 °C, the relative intensity of N–H vibration and –C=C– vibration decreased, and with the temperature arise, the vibration bonds become weaker. It means that the amount of the N–H groups and –C=C– groups decreased by the cross-linked of residual PSN (–Si–N–C–N–Si–), shown in Fig. 3. Notably, the band at 1403 cm^{-1} in PBSN2 was stronger than that in PBSN1. It was attributed to the reaction between BCl_3 with N–H bonds of PBSN1, which was shown in Eq (1). Meanwhile, little BH_3 was involved in the process of the new formation of B–N bonds. This may lead to different relative intensity of B–N vibration between PBSN1 and PBSN2.

In order to clarify the difference among the three types of precursor as the pyrolysis temperature, the FTIR spectroscopy at different temperatures has been investigated as shown in Fig. 4. There is a decrease in the intensity of the absorption bands related to Si–H and C–H bands groups, which indicates the organic functional groups disappears and the valence relationship in inorganics. Meanwhile, the increased intensity of B–N and Si–C functional groups over 1100 °C ascribe to the relative content reduction of the Si_3N_4 decomposition. In addition, FTIR spectroscopy can be applied to compare the boron concentration of these three samples using the same weight measure. The B–N peak area of PBSN2 is larger than that of PBSN2, suggesting larger boron content in PBSN2 which further proves our synthesis route.

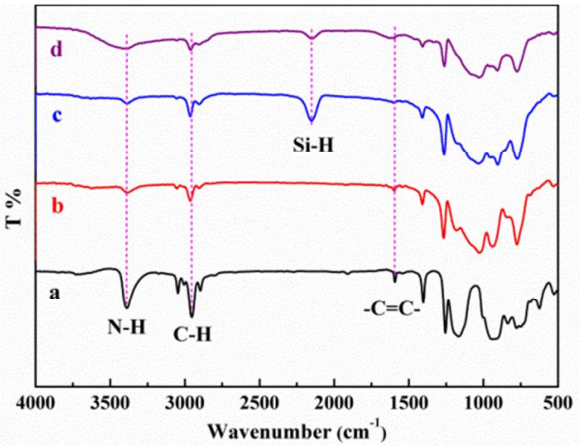

Fig. 5 FTIR spectra of PBSN2 after heat-treatment at different temperatures (a, 100 °C; b, 120 °C; c, 150 °C; d, 180 °C) in the flowing Ar atmosphere.

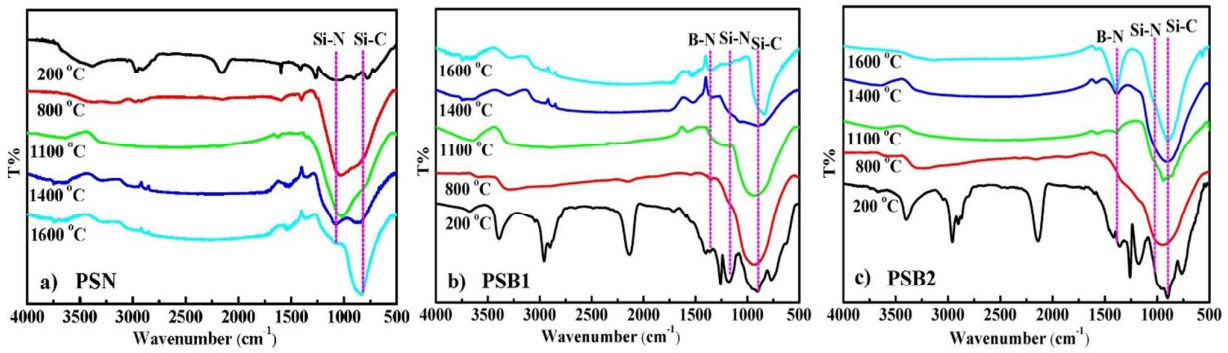

Fig. 4 FTIR spectra of PSN (a), PBSN1 (b) and PBSN2 (c) pyrolyzed at different temperatures.

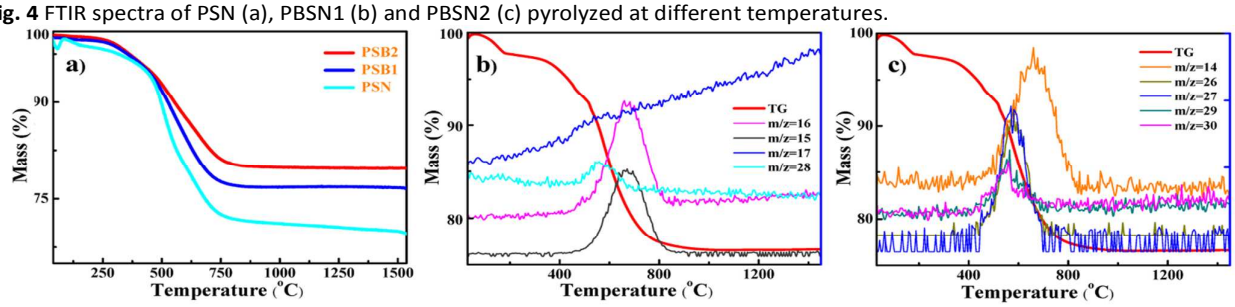

Fig. 6 Thermogravimetric analysis (a) and quadropole-mass spectrometry analysis of cross-linked polysilazane (PSN) modified with BH_3 and BCl_3 to PBSN2 showing the release of (b) CH_4, CH_3, NH_3 and C_2H_4 fragments; (c) CH_2, C_2H_2, C_2H_3, CH_2NH_2, CH_2NH_3 fragments. MS of m/*z* = 44 is shown.

Furthermore, the structural evolution starting from the liquid to cross-linked polymers version was studied exemplarily with the compound PBSN2 by FTIR (Fig. 5). With the temperature increasing from 100 ° to 180 °C, the intensity of Si–H and N–H bands decreased obviously due to the further cross-linking by dehydrocoupling and aminolysis (Si–H/Si–H and Si–H/N–H) (see Eq. 1).[22] The intensity of –C=C– groups was due to the hydroboration and aminolysis (see Eq. 1) reaction.

Pyrolysis behavior of polymeric precursors

TGA-DSC-QMS analyses of PSN, PBSN1 and PBSN2 were run to follow the ceramization process (Fig. 6) (TGA-DSC analysis shown in Fig. S2). All of polymer precursors were cured at 20 °C (above their curing temperatures) with the same dwell time. They have been crosslinked at their own softening point (130 °, 160 ° and 170 °C). Four distinct mass loss events are seen for cross-linked PSN: in the first step, 3 wt% between 25 ° and 200 °C, secondly, 2.4 wt% between 200 ° and 450 °C, thirdly, 22 wt% between 450 ° and 750 °C, and at the last, 3.3 wt% between 750 ° and 1550 °C. Previous results suggested that these mass losses were due to evolution of methane (CH_4) and H_2 along with the evolution of low-molecular-weight oligomers.[17, 22]

In contrast, a three-step mass loss process is observed for PBSN2. Mass loss of solvent and oligomer with 0.9 wt% is observed beyond 800 °C. The 18 wt% mass loss among 300 ° – 800 °C, is primarily due to the release of CH_4, H_2 and molecules containing two or four carbon units.[23] Finally, a 0.5 wt% mass loss likely of H_2 occurs at the highest temperatures, giving a final sample mass of 80 wt%. It suggests that the significant role of boron in cross-linking PSN limits mass loss in the early stage of decomposition for PBSN1 and PBSN2.[22]

Another possible reason for the higher yields could be the enhancement of the cross-linking reaction of hydrosilylation after the introduction of BTC.[22] The thermolysis of starting liquids of PBSN2 was shown in Fig. S5, indicating the curing behavior of the materials. The mass loss of liquid PBSN2 (ca. 25 wt%) is ~5 wt% higher than that of cross-linked PBSN2 precursor. It may due to the left toluene after spinned remain in PBSN2 to reduce 5 wt% ceramic yield of PBSN2. Accordingly, PBSN2 preceramic polymer gives a higher ceramic yield (~80 wt%) than PBSN1 preceramic polymer precursor (76 wt%). While PBSN1 and PBSN2 give higher ceramic yield compare to PSN (70 wt%), which is considered being a consequence of the strong increase of the cross-linking degree of the polymer upon modification with dual-boron source.

These findings conform nicely the results of the TGA-DSC-QMS investigations described below. At higher temperatures, the *v*Si–C, *v*Si–N and *v*B–N separate and become sharper, as successive crystallization of phases separate from the amorphous SiBCN ceramics. Combining solid-state multinuclear (^{29}Si and ^{11}B) NMR and FTIR spectra allows one to propose structures for precursors PBSN1 and PBSN2 based on the reported structure of PSN. Thus BCN_2, BN_3, BC_3 and BC_xN_y (x+y=4) units are not common in microstructures as reported in the literature.

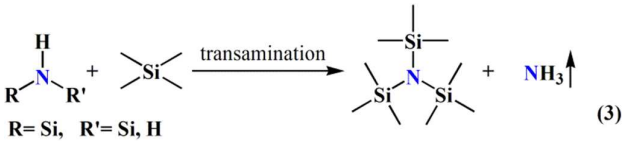

(3)

Quadropole Mass-Spectrometer (QMS) coupled with TGA of PBSN2 were used to support our discussions (Fig. 6b and Fig. 6c).[17,21] The thermolysis of the polyborosilazane is considered to be occurred at the temperature range of 200 ° – 800 °C. The endotherm at 190 °C is attributed to evolution of NH_3 and (CH_x) (x = 1–4, m/z = 13–16) by aminolysis reactions to form oligomeric units (m/z = 17) between PSN and PBSN1. Here, the H_2 evolution starts at 320 °C as a result of dehydrocoupling and transamination reactions of the Si–H/N–H or B–H/N–H groups (see Eq. 3), coincident with evolution of ethane (C_2H_x) (x = 2–6, m/z = 26–30) between 420 ° and 720 °C. However, there is no evolution of NH^+ (m/z = 15) and NH_2^+ (m/z = 16) for the cross-linked boron-rich PBSN2 at the low temperature range of 200 ° – 470 °C. The methanes and hydrocarbons form at 500 ° – 800 °C because of the decomposition of C–C bonds and Si–CH_3 units. This evolution of all hydrosilylation is delayed, and the decomposition of the organic substituents are reduced because of the boron in the backbones of PBSN2 increased the cross-linking density.[3] As mentioned above on TGA-QMS can further illustrate the 5.6–9.7 wt% improved ceramic yield for the boron-modified PSN (Fig. S3 and Fig. S4).

Pyrolyzed ceramics from polymeric precursors

The XPS analysis of the three precursors with different boron contents (PSN, PBSN1, PBSN2) at variable temperatures show Si 2p, N 1s, C 1s and B 1s elemental peaks arising from valence energy levels. The resolution of each peak of PBSN2 (PBSN1 is shown in Fig. S3) determines the corresponding phases and their proportions in the final product, as shown in Fig. 7.

A small broad peak at 190.4 eV is attributed to the B–N bonds, whereas the large peak at 191.5 eV corresponds to more electronegative N–B bonds (as in B–N–C) that associate with vinyl. Furthermore, the results of Gauss-Lorentz formula clearly show that the boron contents in PBSN2 are higher than that in PBSN1. The binding energy of C1s at 284.6 eV corresponds to graphite-like carbon sample surfaces, whereas a lower energy intense peak in the PBSN2 at 283 eV and a broad peak at 283.5 eV in the PBSN1 is due to Si–C bonds of Si 2p. The Si 2p photoelectrons emerge as two distinct peaks at 100.4 eV and 102 eV attribute to SiC and Si_3N_4, respectively. N 1s bonding energies of 397.8 and 398.4 eV indicate Si–N and B–N bonds, respectively. Nevertheless, small amount of Si–N from the precursor is not very obvious after pyrolyzed at 1600 °C. The areas peaks attributable to Si–N bonds decrease with increasing temperatures conforming to the XRD profiles of PBSN1 and PBSN2. Meanwhile, with the increasing temperature, nitride content of PBSN2 decreases. Thereby, SiC, Si_3N_4 and BN appear in both PBSN1 and PBSN2.

A comparison of XPS data in pyrolysis process indicates the different chemical bonds of boron in PBSN2. XPS is crucial in determining the difference between PSN, PBSN1 and PBSN2 at varying pyrolysis temperatures. The percentage of chemical elements constituting PBSN1 and PBSN2 is obtained by XPS.

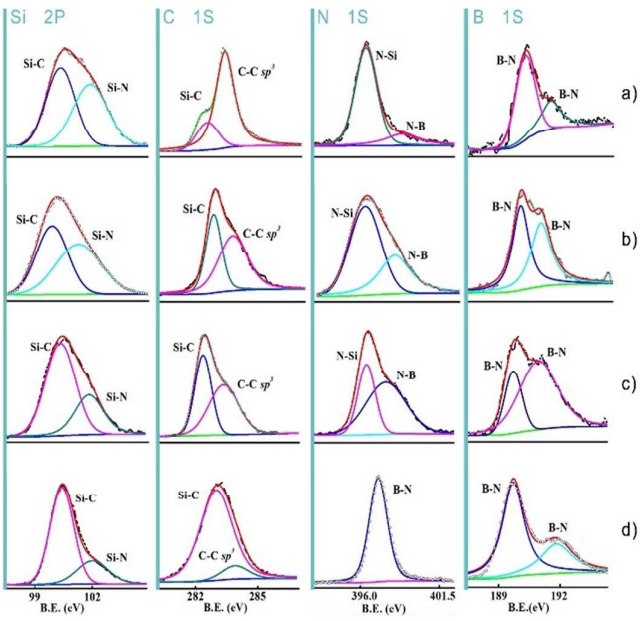

Fig. 7 XPS spectra of PBSN2 pyrolyzed at (a) 800 °C, (b) 1100 °C, (c) 1400 °C and (d) 1600 °C, respectively. The Si–C and B–N content increases with the rising temperature, while Si–N signal is reduced.

The chemical compositions are reported in Table 2, oxygen (content≤ 2 wt%) omitted in the calculation of the empirical formula,[24] from which we learn PBSN1 has higher silicon and boron contents than PBSN2.

Table 2 Chemical Composition (wt%) of PSN, PBSN1 and PBSN2 derived ceramic after thermolysis at varied temperatures (Oxygen has been omitted).

Sample	Atomic and mass fraction (%)				
	Si	C	N	B	Empirical formula
PSN 800	44.31	26.85	28.84	--	$SiC_{2.0340}N_{1.7013}$
PSN 1100	45.28	26.58	28.14	--	$SiC_{2.1197}N_{1.5021}$
PSN 1400	51.89	25.46	22.65	--	$SiC_{2.2005}N_{1.2886}$
PSN 1600	56.20	27.09	16.71	--	$SiC_{2.2554}N_{1.1858}$
PBSN1 800	42.92	23.27	28.51	5.29	$SiC_{1.6876}N_{1.3800}B_{0.4795}$
PBSN1 1100	43.27	23.34	27.74	5.65	$SiC_{2.0773}N_{1.2208}B_{0.5036}$
PBSN1 1400	43.88	23.70	26.49	5.93	$SiC_{2.0406}N_{1.1273}B_{0.5941}$
PBSN1 1600	45.67	24.56	23.52	6.25	$SiC_{2.0331}N_{0.7796}B_{0.4675}$
PBSN2 800	41.57	24.46	23.47	10.54	$SiC_{1.7342}N_{1.3350}B_{0.9739}$
PBSN2 1100	42.25	24.78	22.19	10.78	$SiC_{1.8233}N_{1.1894}B_{0.9960}$
PBSN2 1400	42.92	25.28	21.54	10.76	$SiC_{1.8575}N_{1.1737}B_{0.9942}$
PBSN2 1600	43.09	25.65	20.17	11.09	$SiC_{1.8858}N_{1.0759}B_{1.0247}$

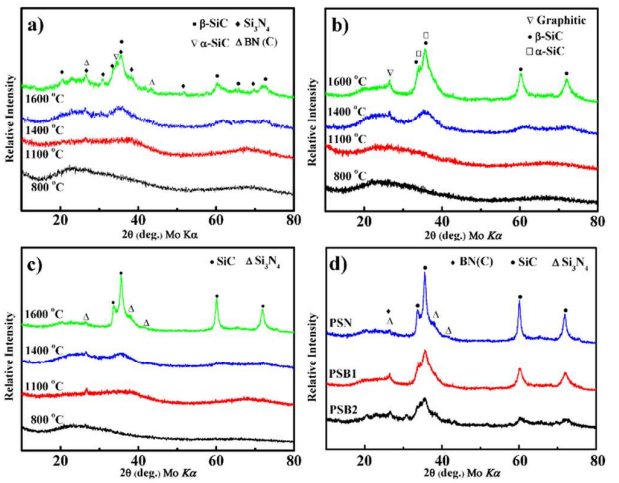

Fig. 8 Crystallization behaviour of precursor-derived ceramic powder upon annealed at temperatures ranges of 800 ° –1600 °C in Ar: (a) PBSN2, (b) PBSN1, (c) PSN. SiBCN ceramics are amorphous till 1400 °C, crystallization was exhibited at 1600

°C. (d) Crystallization behaviour of precursor-derived ceramic powder upon annealed at temperatures 1600 °C.

The pyrolyzed samples are crushed with mortar, then the XRD patterns for PSN, PBSN1 and PBSN2 pyrolyzed in range of 800 ° – 1600 °C are shown in Fig. 8, respectively. No crystallinity is observed from 800 ° to 1300 °C. Three peaks are seen at 2θ = 35.6 °, 60.1 ° and 72 ° for the PSN derived ceramic annealed at 1400 °C, ascribed to formation of β-SiC (1 1 1), (2 2 0) and (3 1 1) planes, respectively. The sample annealed at 1600 °C exhibits broad reflections due to the segregation of nanocrystalline silicide.[25] However, the crystallization is incomplete and the ceramic still maintains predominantly amorphous. Although the ordered temperature is as high as 1600 °C, the reflections are still broad and weak, especially compared with the PSN derived ceramic heating at the same temperature. These peaks of PSN become narrower and more intense as well as the rapid crystallization of SiC, with increasing in annealing temperature, which is shown in Fig. 8c.

The XRD profiles of the PBSN2 presented in Fig. 8a indicate the typical amorphous with diffuse scattering peaks at 2ϑ = 35.6 ° which are assigned to β-SiC (similar result can be found in Fig. 8b). PBSN1 and PBSN2 with higher B contents than PSN, producing SiC, β-Si_3N_4 and BN(C) at higher temperatures described in Fig. 8d. Furthermore, the crystallinity of PBSN1 is higher than PBSN2, and the different ratios of products were due to the increased B content. Then, the most noticeable difference appears in the BCN reflections at 2ϑ = 26.7 °, 41.7 ° (JCPDS card No. 51-768) in XRD patterns of PBSN1 (Fig. 8a) and PBSN2 (Fig. 8b). Interestingly, β-Si_3N_4 crystallite trace was observed between 1100 °C and 1400 °C, while the reflection disappear when the temperature up to 1600 °C (in Fig. 8c). The presence of turbostratic boron nitride is also indicated by small Bragg reflections at 26.4° and 20° at 1600 °C indexed as crystalline BN(C) or graphitic carbon. The above results conform to the XPS analysis. Fig. 8d reveals the XRD patterns of the samples with different boron contents at 1600 °C. Consequently, as the temperature rises, both the boron content and the crystallization temperature increase. Moreover, with higher boron content, the decomposition of Si_3N_4 can be suppressed more effectively to improve the thermostability of silicon carbonitride ceramics.

Conclusions

We reported a novel route to modify the skeletal structure of precursor molecule to effectively improve the boron content of precursor polymer. A series of polymer-derived SiBCN ceramics containing 0, ~5 wt% and ~10 wt% boron contents were obtained after they pyrolysis above 800 °C. The final product with rich boron was synthesized by hydroboration and aminolysis reaction of polysilazane with borane tetrahydrofuran complex and boron trichloride hexane complex, which were subsequently pyrolyzed. The presences of dual-boron resource effect on the molecular structures of polyborosilazanes were examined by solid-state ^{11}B, ^{29}Si MAS NMR, FTIR spectra. The thermal transformation of the both polyborosilazanes into an amorphous SiBCN ceramic was studied by a combination of TGA-DSC coupled with QMS, XPS and XRD as well as FTIR spectra. Both of polyborosilazanes derived ceramics in sufficient yield which possessed excellent thermal degradation and chemical stability, and remained amorphous up to at least 1400 °C. The main crystalline phases after pyrolysis were SiC, Si_3N_4 and BN. The rheological property of precursor polymers and the oxidative stability of the precursor-derived SiBCN ceramics will be studied in the next work. Accordingly, modifications on the molecular level of precursor polymers enable the fabrication of a vast range of advanced ceramics to be applied in numerous engineering and specialized applications such as ceramic fiber, which will be further investigated.

Acknowledgements

The research leading to these results is supported by the National Natural Science Foundation of China (No. 51321061, No. 51472059 and No. 51272300) and China National Funds for Distinguished Young Scientists (No. 51225203). The authors would like to thank the editors and anonymous reviewers for their useful comments and help improve the quality of this paper. The help of Prof. Richard M. Laine for the discussion is gratefully acknowledged.

Notes and references

1 (a) M. Zaheer, T. Schmalz, G. Motz and R. Kempe, *Chem. Soc. Rev.,* 2012, **41**, 5102–5116; (b) R. Bhandavat, W. Kuhn, E. Mansfield, J. Lehman and G. Singh, *ACS Appl. Mater. Interfaces*, 2012, **4**, 11–16; (c) Y. Chen, X. Yang, Y. Cao, Z. Gan and L. An, *Acta Mater.*, 2014, **72**, 22–31; (d) L. David, S Bernard, C. Gervais, P. Miele and G. Singh, *J. Phys. Chem. C*, 2015, **119**, 2783–2791; (e) J. Kong, T. Schmalz, G. Motz, and A. H. E. Müller, *J. Mater. Chem. C*, 2013, **1**, 1507–1514; (f) J. Kong, X. Fan, Q. Si, G. Zhang, S. Wang and X. Wang, *J. Polym. Sci., Part A: Polym. Chem.,* 2006, **44**, 3930–3941; (g) L. Meng, X. Zhang, Y. Tang, K. Su and J. Kong, *Sci. Rep*., 2015, **5**, 7910.

2 (a) W. Lin, K.-S. Moon, S. Zhang, Y. Ding, J. Shang, M. Chen and C. P. Wong, *ACS nano*, 2010, **4**, 1716–1722; (b) L. An, W. Xu, S. Rajagopalan, C. Wang, H. Wang, Y. Fan, L. Zhang, D. Jiang, J. Kapat and L. Chow, *Adv. Mater.,* 2004, **16**, 2036–2040; (c) J. H. Jung, J. Furgal, T. G. Goodson, T. Mizumo, M. Schwartz, K. Chou, J. F. Vonet and R. M. Laine, *Chem. Mater.*, 2012, **24**, 1883–1895; (d) W. S. Kim, S. Y. Moon, N.-H. Park, H. Huh, K. B. Shim and H. Ham, *Chem. Mater.*, 2011, **23**, 940–944; (e) P. Colomb, D. C. Dunand and V. Kumar, *J. Mater. Res.*, 2013, **28**, 2187–2190; (f) Y. H. Chen, X. P. Yang, Y. J. Cao and L. An., *J. Eur. Ceram. Soc.*, 2014, **34**, 2163–2167; (g) L. M. Reinold, Y. Yamada, M. Graczyk–Zajac, H. Munakata, K. Kanamura and R. Riedel, *J Power Sources*, 2015, **282**, 409–415.

3 J. Kong, M. Wang, J. Zou and L. An, *ACS Appl. Mater. Interfaces*, 2015, **7**, 6733–6744.

4 G. Mera, R. Ishikawa, E. Ionescu, Y. Ikuhara and R. Riedel, *J. Eur. Ceram. Soc.*, 2015, **35**, 3355–3362.

5 (a) S. Bernard, M. Weinmann, P. Gerstel, P. Miele and F. Aldinger, *J. Mater. Chem.*, 2005, **15**, 289–299; (b) S. Sarkar, J. Zou, J. Liu, C. Xu, L. An and L. Zhai, *ACS Appl. Mater. Interfaces*, 2010, **2**, 1150–1156. (c) P. Baldus, M. Jansen and D. Sporn, *Science,* 1999, **285**, 699–703; (d) L. Lu, Y. Song and C. Feng, *J. Mater. Sci. Lett.*, 1998, **17**, 599–602; (e) Y. Zhang,

X. Yin, F. Ye and J. Kong, *J. Eur. Ceram. Soc.*, 2014, **34**, 1053–1061; (f) J. Yuan, X. Luan, J. Yuan, X. Luan, R. Riedel and E. Ionescu, *J. Eur. Ceram. Soc.*, 2015, **35**, 3329–3337.

6 (a) P. Dibandjo, L. Bois, F. Chassagneux, D. Cornu, J. M. Letoffe, B. Toury, F. Babonneau and P. Miele, *Adv. Mater.*, 2005, **17**, 571–574; (b) P. Colombo and H. P. Degischer, *Adv. Eng. Mater.*, 2012, **14**, 1051–1051.

7 (a) S. H. Lee and M. Weinmann, *Acta Mater.*, 2009, **57**, 4374–4381; (b) A. Staubitz, A. Presa Soto and I. Manners, *Angew. Chem. Int. Ed.*, 2008, **47**, 6212–6215; (c) C. Schitco, M. S. Bazarjani, R. Riedel and A. Gurlo, *J. Mater. Chem. A*, 2015, **3**, 805–818; (d) P. Colombo, G. Mera, R. Riedel and G. D. Soraru, *J. Am. Ceram. Soc.*, 2010, **93**, 1805–1837.

8 (a) U. Müller, M. Weinmann and M. Jansen, *J. Mater. Chem.*, 2008, **18**, 3671–3679; (b) R. Ngoumeni-Yappi, C. Fasel, R. Riedel, V. Ischenko, E. Pippel, J. Woltersdorf and J. Clade, *Chem. Mater.*, 2008, **20**, 3601–3608; (c) J. Wilfert and M. Jansen, *J. Mater. Chem.*, 2012, **22**, 9782–9786.

9 (a) R. Riedel, A. Kienzle, W. Dressler, L. Ruwisch, J. Bill and F. Aldinger, *Nature*, 1996, **382**, 796; (b) A. Müller, P. Gerstel, M. Weinmann, J. Bill and F. Aldinger, *Chem. Mater.*, 2002, **14**, 3398–3405; (c) S. Sarkar, Z. Gan, L. An and L. Zhai, *J. Phys. Chem. C*, 2011, **115**, 24993–25000; (d) J. Kong, M. Kong, X. Zhang, L. Chen, L. An, *ACS Appl. Mater. Interfaces*, 2013, **5**, 10367–10375.

10 K. Jie, M. Wang, J. Zou and L. An, *Macromol.*, 2011, **44**, 1280–1291.

11 (a) M. Weinmann, M. Kroschel, T. Jäschke, J. Nuss, M. Jansen, G. Kolios, , A. Morillo, C. Tellaeche and U. Nieken, *J. Mater. Chem.*, 2008, **18**, 1810–1818; (b) J. Haberecht, F. Krumeich, H. Grützmacher and R. Nesper, *Chem. Mater.*, 2004, **16**, 418–423; (c) J. Haberecht, R. Nesper and H. Grützmacher, *Chem. Mater.*, 2005, **17**, 2340–2347; (d) A. H. Tavakoli, J. A. Golczewski, J. Bill and A. Navrotsky, *Acta Mater.*, 2012, **60**, 4514–4522.

12 (a) R. Bhandavat and G. Singh, *J. Am. Ceram. Soc.*, 2012, **95**, 1536–1543; (b) Z. Zhang, F. Zeng, J. Han, Y. Luo, and C. Xu, *J. Mater. Sci.*, 2011, **46**, 5940–5947; (c) A. H. Tavakoli, J. A. Golczewski, J. Bill and A. Navrotsky, *Acta Mater.*, 2012, **60**, 4514–4522.

13 (a) C. Zhou, H. Min, L. Yang, M. Chen, Q. Wen and Z. Yu, *J. Eur. Ceram. Soc.*, 2014, **34**, 3579–3589; (b) S. Widgeon, G. Mera, Y. Gao, S. Sen, A. Navrotsky and R. Riedel, *J. Am. Ceram. Soc.*, 2013, **96**, 1651–1659; (c) T. Wideman, E. Cortez, E. E. Remsen, G. A. Zank, P. J. Carroll and L. G. Sneddon, *Chem. Mater.*, 1997, **9**, 2218–2230; (d) G. Singh and R. Bhandavat, U.S. Patent Application, 14/377. 2013, **123**, 2–7.

14 (a) B. T. Holland, L. Abrams and A. Stein, *J. Am. Chem. Soc.*, 1999, **121**, 4308–4309; (b) A. Guerrero-Martínez, J. Pérez-Juste and L. M. Liz-Marzán, *Adv. Mater.*, 2010, **22**, 1182–1195; (c) H. Xing, J. Li, W. Yan, P. Chen, Z. Jin, J. Yu, S. Dai and R. Xu, *Chem. Mater.*, 2008, **20**, 4179–4181.

15 D. Seyferth and G. H. Wiseman, U.S. Patent, 1984, 4482669.

16 C. Gervais, F. Babonneau, L. Ruwisch, R. Hauser and R. Riedel, *Can. J. Chem.*, 2003, **81**, 1359–1369.

17 L. Gottardo, S. Bernard, C. Gervais, M. Weinmann and P. Miele, *J. Mater. Chem.*, 2012, **22**, 17923–17933.

18 (a) F. Berger, A. Mueller, F. Aldinger and K. Mueller, *Z. Anorg. Allg. Chem.*, 2005, **631**, 355–363; (b) T. A. Pham, D.-P. Kim, T.-W. Lim, S.-H. Park, D.-Y. Yang and K.-S. Lee, *Adv. Funct. Mater.*, 2005, **16**, 1235–1241.

19 S. Bernard and P. Miele, *Materials*, 2014, **7**, 7436–7459.

20 J. Yuan, S. Hapis, H. Breitzke, Y. Xu, C. Fasel, H.-J. Kleebe, G. Buntkowsky, R. Riedel and E. Ionescu, *Inorg. Chem.*, 2014, **53**, 10443–10455.

21 A. C. Stowe, W. J. Shaw, J. C. Linehan, B. Schmid and T. Autrey, *Phys. Chem. Chem. Phys.*, 2007, **9**, 1831–1836.

22 B. Papendorf, K. Nonnenmacher, E. Ionescu, H.-J. Kleebe and R. Riedel, *Small*, 2011, 7, 970–978.

23 J. S. Lee, D. P. Butt, R. H. Baney, C. R. Bowers and J. S. Tulenko, *J. Non-Cryst. Solids*, 2005, **351**, 2995–3005.

24 M. S. Bazarjani, H.-J. Kleebe, M. M. Mueller, C. Fasel, M. B. Yazdi, M. A. Gurl and R. Riedel, *Chem. Mater.*, 2011, **23**, 4112–4123.

25 X. Zhang, L. Chen, L. Meng, F. Chen and J. Kong, *Ceram. Int.*, 2014, **40**, 6937–6947.

Manuscript ID: NJ-ART-12-2015-003723

Synthesis and Structural Evolution of Dual-Boron-Source-Modified Polysilazanes Derived SiBCN Ceramics

Qian Zhang， Zhihua Yang,* Dechang Jia,* Qingqing Chen and Yu Zhou

Graphical abstract

A dual-boron-source approach is proposed to enrich the boron content of SiBCN ceramics through the aminolysis and hydroboration reactions.